Editors' Suggestion

Electrical Tuning of Tin-Vacancy Centers in Diamond

Shahriar Aghaeimeibodi,[*,†] Daniel Riedel,[†] Alison E. Rugar,[†] Constantin Dory, and Jelena Vučković

E. L. Ginzton Laboratory, Stanford University, Stanford, California 94305, USA

(Received 2 March 2021; revised 31 March 2021; accepted 7 May 2021; published 3 June 2021)

Group-IV color centers in diamond have attracted significant attention as solid-state spin qubits because of their excellent optical and spin properties. Among these color centers, the tin-vacancy (Sn-V^-) center is of particular interest because its large ground-state splitting enables long spin coherence times at temperatures above 1 K. However, color centers typically suffer from inhomogeneous broadening, which can be exacerbated by nanofabrication-induced strain, hindering the implementation of quantum nodes emitting indistinguishable photons. Although strain and Raman tuning have been investigated as promising tuning techniques to overcome the spectral mismatch between distinct group-IV color centers, other approaches need to be explored to find methods that can offer more localized control without sacrificing emission intensity. Here, we study the electrical tuning of Sn-V^- centers in diamond via the direct-current Stark effect. We demonstrate a tuning range beyond 1.7 GHz. We observe both quadratic and linear dependence on the applied electric field. We also confirm that the tuning effect we observe is a result of the applied electric field and is distinct from thermal tuning due to Joule heating. Stark tuning is a promising avenue toward overcoming detunings between emitters and enabling the realization of multiple identical quantum nodes.

DOI: 10.1103/PhysRevApplied.15.064010

I. INTRODUCTION

Group-IV color centers in diamond have emerged as promising candidates for the implementation of quantum networks [1,2] because they retain their optical coherence when integrated with nanophotonic devices [3–6]. These color centers are inversion symmetric and thus exhibit a vanishingly small permanent electric dipole moment, which mitigates the influence of electric field fluctuations and results in a high frequency stability of their optical transitions [7]. Most notably, the negatively charged silicon-vacancy (Si-V^-) center in diamond has been used to implement several quantum information processing applications [8–10]. However, the relatively small ground-state splitting (GSS) of Si-V^- centers restricts the long spin coherence of this emitter to millikelvin temperatures. On the other hand, the negatively charged tin-vacancy (Sn-V^-) center comprises a heavier group-IV element in a split-vacancy configuration [11–16]. The comparatively large GSS of Sn-V^- centers facilitates long spin coherence times at liquid-helium temperatures (> 1 K) because of the reduced phonon-induced decoherence [17].

Quantum networks require multiple identical quantum nodes that emit indistinguishable photons. A significant challenge for solid-state quantum emitters is that each individual emitter experiences a slightly different strain environment, leading to an inhomogeneous distribution of their optical transition frequencies. Because of the aforementioned inversion symmetry, the spread of optical transition frequencies of group-IV color centers can be very narrow in a low-strain environment [18,19]. Nevertheless, in diamond nanostructures, fabrication-induced strain produces a slightly larger inhomogeneous broadening (< 15 GHz) [5]. Therefore, to achieve indistinguishable emission from distinct color centers, precise tuning of optical transition frequencies is essential. Raman [3,20] and magnetic field [8] tuning have been employed to control the emitter frequency over ranges comparable to this spread. Those techniques, however, either strongly reduce the photon detection rate or cannot be applied locally on several emitters on the same chip to compensate their frequency detuning. Electromechanical tuning offers a potential solution and has enabled the tuning of the transition frequency of waveguide-coupled Si-V^- centers by tens of gigahertz [6,21]. This technique, however, is limited to freestanding waveguide structures. The application of an electric field could potentially offer an alternative tuning mechanism through the Stark effect [22,23]. However, because of the predicted first-order insensitivity of their transitions to electric fields, this approach has not been realized in group-IV diamond color centers.

*shahriar@stanford.edu

†These authors contributed equally to this work.

In this paper, we investigate the electric field susceptibility of Sn-V^- centers in diamond. We demonstrate reversible tuning of the transition frequency by more than 1.7 GHz, an order of magnitude larger than the transition linewidth. We measure the linear and quadratic Stark-effect coefficients for Sn-V^- centers to be several orders of magnitude smaller than those of non-inversion-symmetric color centers. The remaining linear shift in some emitters may originate from the relatively high strain in our diamond sample, which we infer from the large distribution of transition frequencies (approximately 270 GHz) of Sn-V^- centers in this sample, as previously characterized in Ref. [12]. Furthermore, we perform careful control experiments to distinguish the tuning achieved through the Stark effect from that resulting from parasitic heating of the diamond sample. Our results, when combined with an initial preselection of emitters for nearby transition frequencies, could enable the realization of multiemitter quantum information processing applications using diamond color centers.

II. FABRICATION AND CHARACTERIZATION

We begin our fabrication process with an electronic grade single-crystal diamond plate from Element Six. The chip is cleaned in a boiling triacid (1:1:1 sulfuric:nitric:perchloric acids) solution. We then remove the top 300 nm of diamond with an oxygen (O_2) plasma etch. Sn-V^- centers are generated via $^{120}Sn^+$ ion implantation (370 keV, 2×10^{11} cm^{-2}) followed by vacuum annealing at 800 °C for 30 min and 1100 °C for 90 min. Based on the Stopping and Range of Ions in Matter (SRIM) simulations [24], we expect the depth of our Sn-V^- centers to be approximately 90 nm.

After generating Sn-V^- centers in diamond, we fabricate nanopillars and mesas to easily identify single Sn-V^- centers and to increase the photon extraction efficiency. We grow 200 nm of silicon nitride (Si_xN_y) via low-pressure chemical-vapor deposition. We pattern square arrays of circles (pillars) separated by rectangles (mesas) in hydrogen silsesquioxane (FOx-16) via electron-beam (*e*-beam) lithography. The circles range in diameter from 140 nm to 300 nm. The rectangles are 0.2 μm × 2.5 μm. The pattern is transferred into the Si_xN_y film by a SF_6, CH_4, and N_2 reactive ion etch. Using the Si_xN_y layer as an etch mask, we perform an O_2 plasma etch to fabricate 500-nm-tall diamond nanopillars and mesas. Finally, the etch mask is removed by soaking the sample in hydrofluoric acid.

We then fabricate parallel electrodes around a column in an array of nanopillars to produce an electric field along the [100] direction. The 4-μm-wide electrodes are placed 1 μm apart. The electrodes are created via metal liftoff. Poly(methyl methacrylate) (PMMA) is patterned via *e*-beam lithography. Then 5 nm of Ti followed by 30 nm of Au are deposited by *e*-beam evaporation. The remaining PMMA is lifted off in acetone. A scanning-electron-microscope image of the resulting diamond structures and metal electrodes is shown in Fig. 1(a).

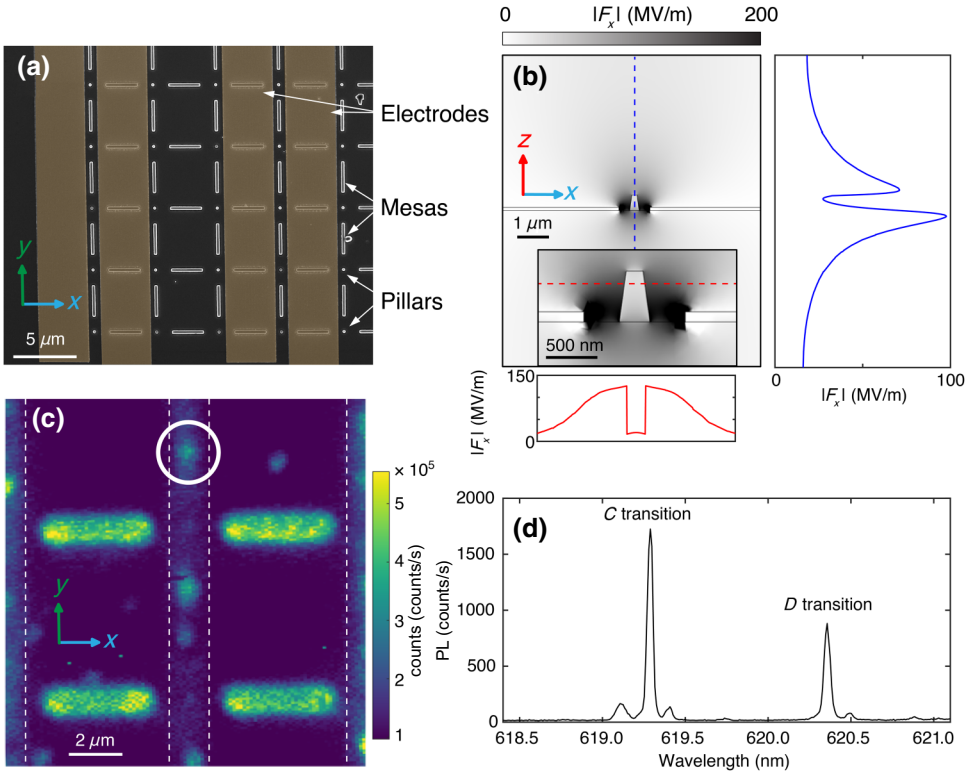

FIG. 1. The device fabrication and characterization. (a) A scanning-electron-microscope image of the fabricated diamond structure and electrodes. The electrodes are highlighted by false-color gold. (b) The simulated electric field magnitude along the x direction ($|F_x|$) for an applied voltage of 200 V across the electrodes. The inset shows a close-up of $|F_x|$ in mesa. The electric fields along the blue and red dashed lines are plotted in the panels to the right ($|F_x(z)|$) and below ($|F_x(x)|$), respectively. (c) The photoluminescence map of the device. One of the Sn-V^- centers that we study in this work (E_1) is circled in white. The edges of the electrodes are demarcated by white dashed lines. (d) The photoluminescence spectrum acquired from the marked Sn-V^- center in (c) at zero applied electric field.

We use the finite-element method (COMSOL) to simulate the electric field inside a pillar or a mesa. Figure 1(b) shows the simulated magnitude of the electric field along the x direction ($|F_x|$) when 200 V is applied across the electrodes. The inset is a close-up view of the field distribution around the mesa, indicating a lower magnitude in the mesa compared to the bulk region. The right panel in Fig. 1(b) is a vertical line cut through the center of a diamond mesa, showing $|F_x|$ as a function of the z position, while the bottom panel shows $|F_x|$ as a function of x at the estimated implantation depth. The electric field magnitude is a factor of 3 smaller at approximately 90 nm below the top of the mesa than at the surface of diamond for a bulk region. Furthermore, the electric field magnitude is approximately 27% higher at the center of a pillar compared to the center of a mesa. However, all the emitters studied in this work are located within mesas.

We perform the optical characterization of Sn-V^- centers in this sample at approximately 5 K in a cryostat (Montana Instruments Cryostation). Using a home-built scanning confocal microscope setup, we scan a 532-nm continuous-wave laser across our sample and collect the emission into the Sn-V^- center zero-phonon line with a (620 ± 14)-nm band-pass filter placed in front of a multimode fiber to acquire a photoluminescence (PL) map of the region [Fig. 1(c)].

To confirm that the fluorescence originates from the Sn-V^- centers, we perform a PL spectroscopy measurement, shown in Fig. 1(d), on the emitter circled in Fig. 1(c), which we will refer to as E_1. At 5 K, the Sn-V^- center has two dominant zero-phonon line transitions, often referred to as the C and D transitions [14]. These transitions are centered around 620 nm and in unstrained Sn-V^- centers the C transition is typically approximately 850 GHz higher in energy than the D transition, which corresponds to the GSS of the emitter.

III. VOLTAGE-DEPENDENT PHOTOLUMINESCENCE EXCITATION

We perform a photoluminescence-excitation (PLE) measurement on the C transition of E_1, to characterize its resonant frequency and linewidth. We scan the wavelength of a tunable laser (MSquared SolsTiS and External Mixing Module) around the transition wavelength at a rate of 0.6 GHz/s and collect the emission into the phonon sideband (PSB) with a 638-nm long-pass filter and a 700-nm short-pass filter placed before a multimode collection fiber. When the laser passes through resonance with the C transition, a peak occurs in the PSB photon counts.

To investigate the behavior of the Sn-V^- center in the presence of an electric field, we apply a direct-current (dc) voltage to the electrodes using a high-voltage power supply (Stanford Research Systems PS325). Figure 2(a) shows consecutive PLE scans of the color center E_1 as we vary the applied voltage. We observe a reversible red shift in the resonant frequency of the Sn-V^- center for both polarities of the electric field. Repeatable tuning of the emission frequency confirms that there is no damage to the Sn-V^- center even at extremely high electric fields of approximately 50 MV/m.

To gain a better understanding of the origin of the shift for single Sn-V^- centers, we fit the PLE data in Fig. 2 to a Lorentzian function to extract the shift, linewidth, and intensity of the signal as we vary the electric field. Figure 2(b) shows close-up views of the PLE spectra for three representative voltages along with the obtained linewidths. We approximate the electric field at

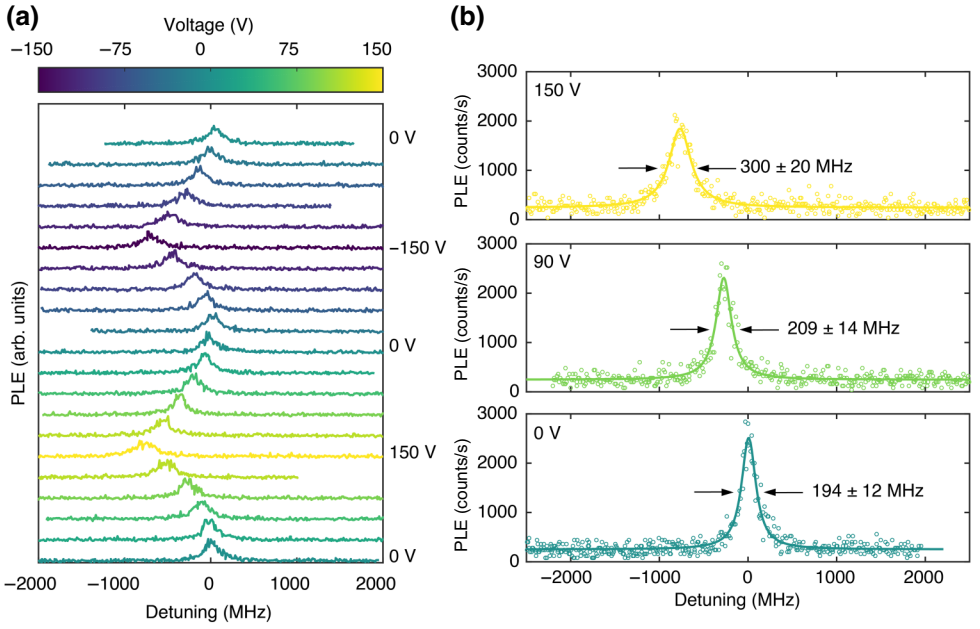

FIG. 2. (a) PLE measurements acquired consecutively at different applied voltages. The PLE resonance reproducibly shifts as a function of applied voltage. (b) Enlarged PLE spectra for three representative voltages. The PLE spectrum (circles) at each voltage is fitted to a Lorentzian function (solid lines).

the location of the emitter using the Lorentz approximation $F_{\text{local}} = F_{\text{ext}}(\epsilon + 2)/3$, where F_{ext} is the field extracted from the COMSOL simulations and ϵ is the dielectric constant of diamond [22].

A. Quadratic shift

Figure 3(a) shows the extracted shift of the resonance frequency of the Sn-V^- center E_1 as a function of the applied electric field. We fit the extracted shift (ΔE) in Fig. 3(a) to a quadratic function of the form $\Delta E = -\Delta\mu F_{\text{local}} - 1/2\Delta\alpha F_{\text{local}}^2$, where $\Delta\mu$ and $\Delta\alpha$ are the change in dipole moment and polarizability between the excited and ground states. An inversion-symmetric defect such as the Sn-V^- center is expected to have a vanishing $\Delta\mu$, making polarizability $\Delta\alpha$ the predominant coefficient. From the fit, we extract $\Delta\mu = (0.97 \pm 0.57)$ MHz/(MV/m), which corresponds to $(1.9 \pm 1.1) \times 10^{-4}$ D. This value is several orders of magnitude smaller

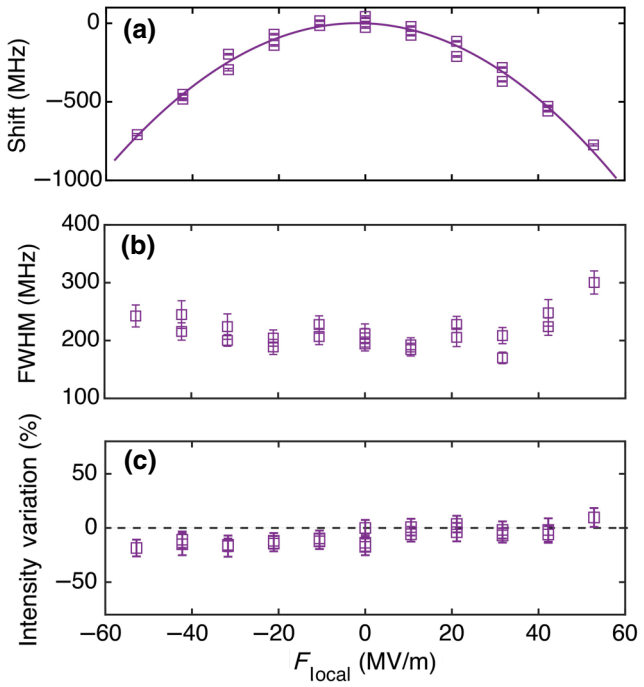

FIG. 3. Characterization of the Stark effect in a single Sn-V^- center (E_1) with a predominantly quadratic shift. (a) The Stark shift extracted from Lorentzian fits to the PLE data in Fig. 2 as a function of the applied electric field F_{local}. The shifts show a mostly quadratic dependence on the applied field, with $\Delta\mu = (1.9 \pm 1.1) \times 10^{-4}$ D and $\Delta\alpha/(4\pi\epsilon_0) = (3.28 \pm 0.18)$Å^3 obtained from the fit. (b) The full width at half maximum (FWHM) of the PLE signal of the same emitter as a function of F_{local}. At high electric fields, the linewidth increases to approximately 300 MHz from its original value of approximately 200 MHz value at zero field. (c) The integrated intensity of the PLE data as a function of F_{local}. We observe $< \pm 20\%$ variation in the integrated intensity of the PLE signal for the entire range of the electric field.

than that of non-inversion-symmetric color centers such as nitrogen-vacancy (N-V^-) centers in diamond [22], chromium-based color centers in diamond [23], and silicon vacancy (V_{Si}) and divacancy centers in silicon carbide [25,26]. We also obtain $\Delta\alpha = (0.55 \pm 0.03)$ MHz/(MV/m)^2, which converts to a polarizability volume $\Delta\alpha/(4\pi\epsilon_0) = (3.28 \pm 0.18)$Å^3. We note that this polarizability volume is 4 orders of magnitude smaller compared to that of N-V^- centers in diamond [22]. Most emitters have a positive polarizability because excited states tend to be more polarizable than ground states; for example, quantum dots [27,28], emitters in two-dimensional materials [29], and molecules [30,31]. Meanwhile, nitrogen-vacancy color centers in diamond exhibit a negative polarizability [22], while for chromium-based color centers both polarities of polarizability have been reported [23]. We note that higher-order Stark-effect coefficients are not required to capture the dependency of Stark shift on the applied electric field. This can be understood by the fact that higher-order hyperpolarizabilities are smaller by a factor of $r = F_{\text{local}}/F_{\text{internal}}$. This ratio of the applied external electric field to the internal electric field of the defect is typically less than 10^{-3} [30].

Figure 3(b) shows the linewidth of the Sn-V^- center obtained from the full width at half maximum (FWHM) of the Lorentzian fits to the PLE data as a function of the applied electric field. We observe an increase in the linewidth from the zero-field value of approximately 200 MHz to 300 MHz for the highest electric field. We attribute this increase in linewidth to the leakage current in the device either through trapped excess charges or a small amount of Joule heating. The broadening of the zero-field linewidth may be caused by strain fluctuations due to the presence of nanofabricated structures [21,32]. The electric field fluctuations in our sample would have to be extremely large (approximately 25 MV/m) to explain the broadening for Sn-V^- center E_1. Figure 3(c) displays the variation in the integrated intensity of the PLE signal as a function of the applied electric field. We observe less than $\pm 20\%$ variation in the integrated intensity of the signal for a large range of applied electric fields, indicating the potential of this technique as a means of tuning Sn-V^- centers into resonance with each other.

B. Linear shift

We study the electric field dependence of the transition frequency for several other Sn-V^- centers. Although a quadratic shift is expected because of the inversion-symmetric structure of this color center, some emitters exhibit a mostly linear shift in transition frequency as a function of the applied electric field. Figures 4(a)–4(c) respectively display the extracted shift, linewidth, and intensity variation of PLE spectra for an emitter with a mostly linear shift (E_2). At local electric field magnitudes

greater than 40 MV/m (shaded blue regions), we observe a red shift in the transition frequency and a sharp increase in the Sn-V^- linewidth regardless of the field polarity. We attribute this linewidth broadening to Joule heating through leakage current. We observe that the onset voltage for the Joule heating decreases over time, indicating a damaged or burned area on the electrodes. Joule heating is less significant for measurements on E_1 in Fig. 3 because those measurements are performed at earlier times with less leakage current. A Joule-heating simulation (COMSOL) shows that because of the high thermal conductivity of diamond, the chip thermalizes quickly and temperature variation on the sample surface is negligible. In order to extract the Stark parameters without distortions caused by heating, we exclude the data in the shaded region for the fit. The solid blue line in Fig. 4(a) is a fit to the same model as in Fig. 3(a) with extracted parameters $\Delta\mu = (3.9 \pm 0.4) \times 10^{-3}$ D and $\Delta\alpha/(4\pi\epsilon_0) = (1.19 \pm 0.89)$ Å^3. This $\Delta\mu$ is more than an order of magnitude larger than that of E_1 studied in Fig. 3 and could be due to broken inversion symmetry in a strained Sn-V^- center. The larger GSS in E_2 (approximately 983 GHz) compared to E_1 (approximately 820 GHz) is another indication of a higher-strain environment for E_2 [33]. We repeat this measurement for multiple Sn-V^- centers between the electrodes and report the extracted parameters in Table I. Also included in the table is the tuning range ("Range") achieved before broadening the linewidth by a factor of 2.

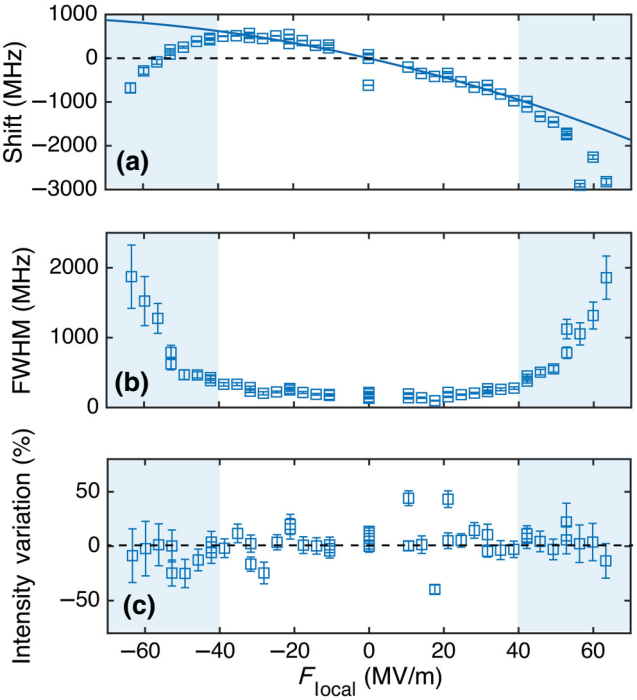

FIG. 4. Characterization of the Stark effect in a single Sn-V^- center (E_2) with a predominantly linear shift. (a) The Stark shift extracted from Lorentzian fits to the voltage-dependent PLE spectra of E_2. The shifts show a mostly linear dependence on the applied field, with $\Delta\mu = (3.9 \pm 0.4) \times 10^{-3}$ D and $\Delta\alpha/(4\pi\epsilon_0) = (1.19 \pm 0.89)$ Å^3 obtained from the fit. (b) The FWHM of the PLE signal of the same emitter as a function of electric field F_{local}. At high electric fields (shaded area), the linewidth increases rapidly. We attribute this significant line broadening to Joule heating through leakage current, as we discuss later in the text. (c) The integrated intensity of the PLE data as a function of F_{local}. We observe $< \pm 45\%$ variation in the integrated intensity of the PLE signal for the entire range of the electric field.

C. Joule heating

To confirm that the observed Stark shift is not related to Joule heating of the color center because of the leakage current, we perform two additional control experiments: we tune a Sn-V^- center either (1) by applying a voltage across the electrodes while measuring an emitter outside of the electrode region (E_{out}) or (2) by heating the sample and studying E_1. We extract the linewidth and resonance frequency of the Sn-V^- centers through PLE measurements. In our first control experiment, we study another emitter E_{out} that is located outside of the electrode region. Because E_{out} is sufficiently far from the electrodes, the dc electric field vanishes and any shift in frequency for this emitter should be due to leakage current, Joule heating, and the high thermal conductivity of diamond. In Figs. 5(a) and 5(b), we plot the shift and FWHM as functions of the square of the voltage applied across the electrodes (V^2).

TABLE I. The linear and quadratic Stark-effect coefficients of single Sn-V^- centers. The wavelength of the C transition, λ_C, and the linewidth are obtained from Lorentzian fits to the PLE spectra at zero electric field. $\Delta\mu$ and $\Delta\alpha$ are Stark coefficients resulting from the same quadratic fit as in Fig. 3(a). The energy difference between the C and D transitions measured through PL spectroscopy at 5 K and zero applied electric field gives the GSS. We define the useful shifting range as the largest tuning range achievable without broadening the linewidth by more than a factor of 2. The transition frequencies of E_1 and E_3 are < 1 GHz apart.

No.	λ_C (nm)	Linewidth (MHz)	$\Delta\mu$ (10^{-3}D)	$\Delta\alpha/(4\pi\epsilon_0)$(Å^3)	GSS (GHz)	Range (GHz)	Type
E_1	619.254	194 ± 12	0.19 ± 0.11	3.28 ± 0.18	819.6	0.82	Quadratic
E_2	619.236	132 ± 6	3.9 ± 0.4	1.19 ± 0.89	982.9	1.68	Linear
E_3	619.255	126 ± 6	-0.5 ± 0.5	3.8 ± 1.1	947.7	0.59	Quadratic
E4	619.500	160 ± 9	-8.2 ± 1.8	5.36 ± 4.05	989.4	1.73	Linear

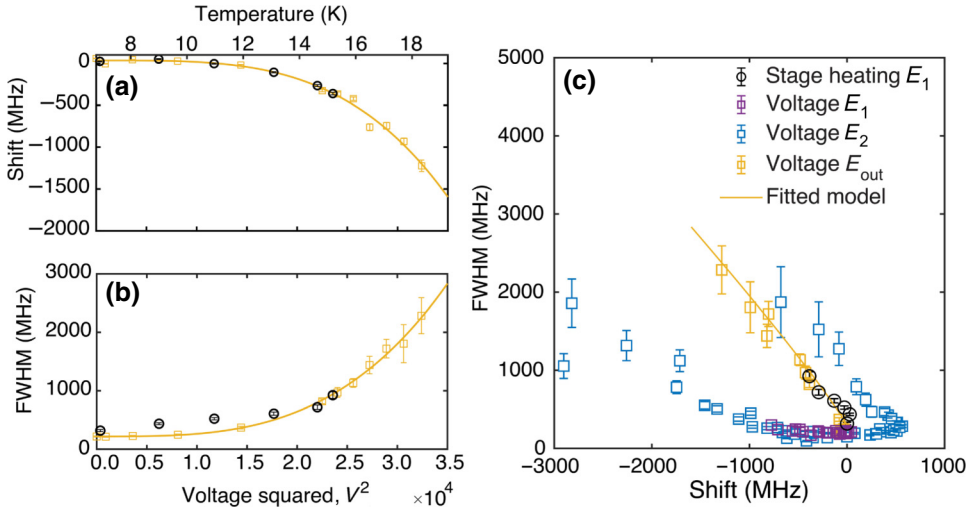

FIG. 5. A comparison between Stark and temperature tuning. (a) The effect of Joule heating on the resonant frequency shift of an emitter E_{out} located outside the electrodes. A power-law model (yellow curve) is fitted to the data (yellow squares), indicating a dependence on temperature ($T \propto V^2$), $T^{3.6\pm0.7}$. The black circles correspond to the temperature-dependent shift for E_1 obtained from heating the sample. (b) The effect of Joule heating on the FWHM of E_{out}. A power-law model (curve) is fitted to the data (squares) with a $T^{3.3\pm0.4}$ dependence on temperature. The black circles correspond to the temperature-dependent FWHM for E_1 obtained from heating the sample. (c) The FWHM as a function of the extracted shift in the PLE signal for three different tuning methods. The purple (blue) squares correspond to the Stark tuning of the emitter E_1 (E_2). The yellow squares show the data for E_{out}. The black circles represent the tuning of emitter E_1 obtained by heating the sample stage. The similar behavior of the black circles and yellow squares confirms that they both originate from heating and are fundamentally different from the shift obtained by the Stark effect. The yellow solid line is the curve resulting from the fitted models from (a) and (b) plotted against each other.

With Joule heating, the induced temperature change is proportional to the square of the applied voltage ($T \propto V^2$), so we use these data to characterize the temperature-dependent behavior of E_{out}. We fit a power-law model to the E_{out} data of Figs. 5(a) and 5(b). From these fits, we find that the thermally induced shift is proportional to $T^{3.6\pm0.7}$ and FWHM goes as $T^{3.3\pm0.4}$. This temperature dependence of the frequency and FWHM is consistent with previous studies of Si-V^- centers [34]. The model of second-order electron-phonon processes presented in the previous study [34] predicts a cubic dependence of both the linewidth and the frequency shift of the optical transition as a function of the temperature. We note, however, that the authors' model for the linewidth broadening is assumed to be only valid for temperatures $T > \mathrm{GSS}/k_B$. An alternative model for explaining a T^3 dependence of the linewidth is based on the fluctuating electric fields that are created as phonons modulate the distance between the color centers and other defects in the crystal [35]. For the second control experiment, we tune the energy of the Sn-V^- center studied in Fig. 3 (E_1) by heating the cryostat up to approximately 20 K. We plot the detuning and FWHM data of E_1 as a function of the temperature in Figs. 5(a) and 5(b). We use the extracted shift of the heated E_1 and E_{out} to calibrate the proportionality constant between V^2 and T.

In Fig. 5(c), we plot the FWHM as a function of the frequency shift for our two control experiments as well as E_1 (Fig. 3) and E_2 (Fig. 4). We also plot the modeled FWHM against the modeled shift from Figs. 5(a) and 5(b) as a solid yellow line. The data from the two temperature-tuning control experiments are consistent with each other and exhibit a vastly different behavior from the electrically tuned E_1. Furthermore, we can see that at large detunings the slope of the E_2 data increases dramatically, approaching the behavior of the thermally tuned emitters. These comparisons prove that while leakage current through electrodes can, in principle, cause Joule heating and broadening of the PLE data, the Stark shifts presented in Figs. 3(a) and 4(a) are not influenced by this effect until very high local fields, exceeding 40 MV/m.

IV. CONCLUSIONS

We examine the response of the frequency of the C transition of Sn-V^- centers in diamond to externally applied electric fields. We can shift the transition frequency by more than 1.7 GHz without introducing a significant broadening of the transition linewidth. We investigate several Sn-V^- centers and observe both linear and quadratic dependencies of the shift on the applied electric field. While a quadratic dependence is expected based on the inversion symmetry of the defect, we attribute the linear shift to a small strain-induced dipole moment. A similar effect has been observed for centrosymmetric molecules

embedded in a polymer matrix [36,37]. We find changes in dipole moment and polarizability volume between the excited and ground states of up to $\Delta\mu = -8.2 \times 10^{-3}$ D and $\Delta\alpha/(4\pi\epsilon_0) = 5.4$ Å^3, respectively. Furthermore, we confirm that the observed shift is due to the Stark effect and is distinct from any heating effects by comparing the linewidth versus frequency shift of the emitter when a voltage is applied to that when the stage is heated.

Stark tuning can be used to tune the optical frequency of remote emitters and to control the degree of indistinguishability in two-photon interference experiments of preselected emitters [38–42]. This technique, which has recently enabled the first demonstration of linking three remote N-V^- centers in a quantum network [43], may also be applied to group-IV color centers. Group-IV color centers have a very narrow inhomogeneous distribution in bulk [18,19] and, because of their inversion symmetry, can also have relatively narrow inhomogeneous distributions in nanostructures (< 15 GHz) [5]. Nanophotonic devices hosting two Si-V^- centers with a subgigahertz difference between their transition frequencies have been reported [8], which is within our Stark tuning range. On this chip, we also observe subgigahertz frequency detuning between two Sn-V^- centers (see Table I). The 1.7 GHz tuning range that we demonstrate in this paper is large enough to overcome modest detunings between color centers and to enable multiemitter experiments.

The electric field dependence of group-IV color centers can be harnessed in other schemes. Modulated electric fields have been proposed as an alternative way to overcome the inhomogeneous broadening of emitters [25,44]. This approach would be particularly important for overcoming detunings between closely spaced emitters; for example, if the emitters are in the same nanophotonic cavity [25,44]. Spectral diffusion presents a challenge when working with group-IV color centers, which require resonant drive for optical spin initialization and control schemes. Feedback-based electric field tuning constitutes a tool for the dynamic stabilization of the optical transition frequency of emitters [45].

All of these applications of Stark-effect-based tuning can be made into more practical options by increasing the achievable Stark tuning range. The Stark tuning range can be further expanded by changing the electrode configuration to increase the field experienced by the emitter. The fabrication of electrodes with a narrower gap between them would increase the applied field. The embedding of the Sn-V^- center below the plane of the electrodes rather than in a nanopillar would increase the field experienced by the emitter a factor of 3. Furthermore, the tuning range can be increased by reducing the voltage-induced heating, which allows the application of larger voltages.

In addition to contributing to a deeper understanding of the basic properties of Sn-V^- centers, our results pave the way for multiemitter experiments based on group-IV color centers harnessing Stark shift tuning.

ACKNOWLEDGMENTS

We are grateful to Daniil Lukin for his experimental assistance. This work is financially supported by the Army Research Office (ARO) (Award No. W911NF-13-1-0309); the National Science Foundation (NSF) Research Advanced by Interdisciplinary Science and Engineering (RAISE)−Transformational Advances in Quantum Systems (TAQS) effort (Award No. 1838976); and the Air Force Office of Scientific Research (AFOSR) Defense University Research Instrumentation Program (DURIP) (Award No. FA9550-16-1-0223). S.A. acknowledges support from the Bloch postdoctoral fellowship in quantum science and engineering from Stanford Q-FARM. D.R. acknowledges support from the Swiss National Science Foundation (Project No. P400P2_194424). A.E.R. acknowledges support from the National Defense Science and Engineering Graduate (NDSEG) Fellowship Program, sponsored by the Air Force Research Laboratory (AFRL), the Office of Naval Research (ONR), and the Army Research Office (ARO). C.D. acknowledges support from the Andreas Bechtolsheim Stanford Graduate Fellowship (SGF) and the Microsoft Research Ph.D. Fellowship. Part of this work was performed at the Stanford Nanofabrication Facility (SNF) and the Stanford Nano Shared Facilities (SNSF), supported by the National Science Foundation under Award No. ECCS-2026822.

Note added.—Recently, we became aware of a similar work [46].

[1] H. J. Kimble, The quantum Internet, Nature **453**, 1023 (2008).
[2] S. Wehner, D. Elkouss, and R. Hanson, Quantum Internet: A vision for the road ahead, Science **362**, eaam9288 (2018).
[3] A. Sipahigil, R. E. Evans, D. D. Sukachev, M. J. Burek, J. Borregaard, M. K. Bhaskar, C. T. Nguyen, J. L. Pacheco, H. A. Atikian, C. Meuwly, R. M. Camacho, F. Jelezko, E. Bielejec, H. Park, M. Lončar, and M. D. Lukin, An integrated diamond nanophotonics platform for quantum-optical networks, Science **354**, 847 (2016).
[4] A. E. Rugar, C. Dory, S. Aghaeimeibodi, H. Lu, S. Sun, S. D. Mishra, Z.-X. Shen, N. A. Melosh, and J. Vučković, Narrow-Linewidth tin-vacancy centers in a diamond waveguide, ACS Photonics **7**, 2356 (2020).
[5] R. E. Evans, A. Sipahigil, D. D. Sukachev, A. S. Zibrov, and M. D. Lukin, Narrow-Linewidth Homogeneous Optical Emitters in Diamond Nanostructures via Silicon Ion Implantation, Phys. Rev. Appl. **5**, 044010 (2016).
[6] N. H. Wan, T.-J. Lu, K. C. Chen, M. P. Walsh, M. E. Trusheim, L. De Santis, E. A. Bersin, I. B. Harris, S. L. Mouradian, I. R. Christen, E. S. Bielejec, and D. Englund,

Large-scale integration of artificial atoms in hybrid photonic circuits, Nature **583**, 226 (2020).

[7] G. Thiering and A. Gali, *Ab initio* Magneto-Optical Spectrum of Group-IV Vacancy Color Centers in Diamond, Phys. Rev. X **8**, 021063 (2018).

[8] R. E. Evans, M. K. Bhaskar, D. D. Sukachev, C. T. Nguyen, A. Sipahigil, M. J. Burek, B. Machielse, G. H. Zhang, A. S. Zibrov, E. Bielejec, H. Park, M. Lončar, and M. D. Lukin, Photon-mediated interactions between quantum emitters in a diamond nanocavity, Science **362**, 662 (2018).

[9] C. T. Nguyen, D. D. Sukachev, M. K. Bhaskar, B. Machielse, D. S. Levonian, E. N. Knall, P. Stroganov, R. Riedinger, H. Park, M. Lončar, and M. D. Lukin, Quantum Network Nodes Based on Diamond Qubits with an Efficient Nanophotonic Interface, Phys. Rev. Lett. **123**, 183602 (2019).

[10] M. K. Bhaskar, R. Riedinger, B. Machielse, D. S. Levonian, C. T. Nguyen, E. N. Knall, H. Park, D. Englund, M. Lončar, D. D. Sukachev, and M. D. Lukin, Experimental demonstration of memory-enhanced quantum communication, Nature **580**, 60 (2020).

[11] U. Wahl, J. G. Correia, R. Villarreal, E. Bourgeois, M. Gulka, M. Nesládek, A. Vantomme, and L. M. Pereira, Direct Structural Identification and Quantification of the Split-Vacancy Configuration for Implanted Sn in Diamond, Phys. Rev. Lett. **125**, 45301 (2020).

[12] A. E. Rugar, C. Dory, S. Sun, and J. Vučković, Characterization of optical and spin properties of single tin-vacancy centers in diamond nanopillars, Phys. Rev. B **99**, 205417 (2019).

[13] A. E. Rugar, H. Lu, C. Dory, S. Sun, P. J. McQuade, Z.-X. Shen, N. A. Melosh, and J. Vučković, Generation of tin-vacancy centers in diamond via shallow ion implantation and subsequent diamond overgrowth, Nano Lett. **20**, 1614 (2020).

[14] T. Iwasaki, Y. Miyamoto, T. Taniguchi, P. Siyushev, M. H. Metsch, F. Jelezko, and M. Hatano, Tin-Vacancy Quantum Emitters in Diamond, Phys. Rev. Lett. **119**, 253601 (2017).

[15] J. Görlitz, D. Herrmann, G. Thiering, P. Fuchs, M. Gandil, T. Iwasaki, T. Taniguchi, M. Kieschnick, J. Meijer, M. Hatano, A. Gali, and C. Becher, Spectroscopic investigations of negatively charged tin-vacancy centres in diamond, New J. Phys. **22**, 013048 (2020).

[16] A. E. Rugar, S. Aghaeimeibodi, D. Riedel, C. Dory, H. Lu, P. J. McQuade, Z.-X. Shen, N. A. Melosh, and J. Vučković, A Quantum Photonic Interface for Tin-Vacancy Centers in Diamond, arXiv: 2102.11852 (2021).

[17] M. E. Trusheim *et al.*, Transform-Limited Photons From a Coherent Tin-Vacancy Spin in Diamond, Phys. Rev. Lett. **124**, 023602 (2020).

[18] L. Rogers, K. Jahnke, T. Teraji, L. Marseglia, C. Müller, B. Naydenov, H. Schauffert, C. Kranz, J. Isoya, L. McGuinness, and F. Jelezko, Multiple intrinsically identical single-photon emitters in the solid state, Nat. Commun. **5**, 4739 (2014).

[19] A. Sipahigil, K. D. Jahnke, L. J. Rogers, T. Teraji, J. Isoya, A. S. Zibrov, F. Jelezko, and M. D. Lukin, Indistinguishable Photons from Separated Silicon-Vacancy Centers in Diamond, Phys. Rev. Lett. **113**, 113602 (2014).

[20] S. Sun, J. L. Zhang, K. A. Fischer, M. J. Burek, C. Dory, K. G. Lagoudakis, Y.-K. Tzeng, M. Radulaski, Y. Kelaita, A. Safavi-Naeini, Z.-X. Shen, N. A. Melosh, S. Chu, M. Lončar, and J. Vučković, Cavity-Enhanced Raman Emission from a Single Color Center in a Solid, Phys. Rev. Lett. **121**, 083601 (2018).

[21] B. Machielse, S. Bogdanovic, S. Meesala, S. Gauthier, M. J. Burek, G. Joe, M. Chalupnik, Y. I. Sohn, J. Holzgrafe, R. E. Evans, C. Chia, H. Atikian, M. K. Bhaskar, D. D. Sukachev, L. Shao, S. Maity, M. D. Lukin, and M. Lončar, Quantum Interference of Electromechanically Stabilized Emitters in Nanophotonic Devices, Phys. Rev. X **9**, 031022 (2019).

[22] P. Tamarat, T. Gaebel, J. R. Rabeau, M. Khan, A. D. Greentree, H. Wilson, L. C. L. Hollenberg, S. Prawer, P. Hemmer, F. Jelezko, and J. Wrachtrup, Stark Shift Control of Single Optical Centers in Diamond, Phys. Rev. Lett. **97**, 083002 (2006).

[23] T. Müller, I. Aharonovich, L. Lombez, Y. Alaverdyan, A. N. Vamivakas, S. Castelletto, F. Jelezko, J. Wrachtrup, S. Prawer, and M. Atatüre, Wide-range electrical tunability of single-photon emission from chromium-based colour centres in diamond, New J. Phys. **13**, 075001 (2011).

[24] J. F. Ziegler, M. Ziegler, and J. Biersack, SRIM—The stopping and range of ions in matter (2010), Nucl. Instrum. Methods Phys. Res. Sect. B: Beam Interact. Mater. At. **268**, 1818 (2010).

[25] D. M. Lukin, A. D. White, R. Trivedi, M. A. Guidry, N. Morioka, C. Babin, Ö. O. Soykal, J. Ul-Hassan, N. T. Son, T. Ohshima, P. K. Vasireddy, M. H. Nasr, S. Sun, J.-P. W. MacLean, C. Dory, E. A. Nanni, J. Wrachtrup, F. Kaiser, and J. Vučković, Spectrally reconfigurable quantum emitters enabled by optimized fast modulation, Npj Quantum Inf. **6**, 80 (2020).

[26] C. F. de las Casas, D. J. Christle, J. Ul Hassan, T. Ohshima, N. T. Son, and D. D. Awschalom, Stark tuning and electrical charge state control of single divacancies in silicon carbide, Appl. Phys. Lett. **111**, 262403 (2017).

[27] S. A. Empedocles, Quantum-confined Stark effect in single CdSe nanocrystallite quantum dots, Science **278**, 2114 (1997).

[28] S. Aghaeimeibodi, C.-M. Lee, M. A. Buyukkaya, C. J. K. Richardson, and E. Waks, Large Stark tuning of InAs/InP quantum dots, Appl. Phys. Lett. **114**, 071105 (2019).

[29] G. Noh, D. Choi, J. H. Kim, D. G. Im, Y. H. Kim, H. Seo, and J. Lee, Stark tuning of single-photon emitters in hexagonal boron nitride, Nano Lett. **18**, 4710 (2018).

[30] C. Brunel, P. Tamarat, B. Lounis, J. C. Woehl, and M. Orrit, Stark effect on single molecules of dibenzanthanthrene in a naphthalene crystal and in a *n*-hexadecane Shpol'skii matrix, J. Phys. Chem. A **103**, 2429 (1999).

[31] R. M. Macfarlane, Optical Stark spectroscopy of solids, J. Lumin. **125**, 156 (2007).

[32] C. T. Nguyen, D. D. Sukachev, M. K. Bhaskar, B. Machielse, D. S. Levonian, E. N. Knall, P. Stroganov, C. Chia, M. J. Burek, R. Riedinger, H. Park, M. Lončar, and M. D. Lukin, An integrated nanophotonic quantum register based on silicon-vacancy spins in diamond, Phys. Rev. B **100**, 165428 (2019).

[33] S. Meesala, Y.-I. Sohn, B. Pingault, L. Shao, H. A. Atikian, J. Holzgrafe, M. Gündoğan, C. Stavrakas, A. Sipahigil,

C. Chia, R. Evans, M. J. Burek, M. Zhang, L. Wu, J. L. Pacheco, J. Abraham, E. Bielejec, M. D. Lukin, M. Atatüre, and M. Lončar, Strain engineering of the silicon-vacancy center in diamond, Phys. Rev. B **97**, 205444 (2018).

[34] K. D. Jahnke, A. Sipahigil, J. M. Binder, M. W. Doherty, M. Metsch, L. J. Rogers, N. B. Manson, M. D. Lukin, and F. Jelezko, Electron-phonon processes of the silicon-vacancy centre in diamond, New J. Phys. **17**, 043011 (2015).

[35] V. Hizhnyakov and P. Reineker, Optical dephasing in defect-rich crystals, J. Chem. Phys. **111**, 8131 (1999).

[36] I. Gerhardt, G. Wrigge, and V. Sandoghdar, Control and imaging of single-molecule spectral dynamics using a nano-electrode, Mol. Phys. **107**, 1975 (2009).

[37] M. Bauer and L. Kador, Electric-field effects of two-level systems observed with single-molecule spectroscopy, J. Chem. Phys. **118**, 9069 (2003).

[38] H. Bernien, L. Childress, L. Robledo, M. Markham, D. Twitchen, and R. Hanson, Two-Photon Quantum Interference from Separate Nitrogen Vacancy Centers in Diamond, Phys. Rev. Lett. **108**, 043604 (2012).

[39] A. Sipahigil, M. L. Goldman, E. Togan, Y. Chu, M. Markham, D. J. Twitchen, A. S. Zibrov, A. Kubanek, and M. D. Lukin, Quantum Interference of Single Photons from Remote Nitrogen-Vacancy Centers in Diamond, Phys. Rev. Lett. **108**, 143601 (2012).

[40] R. Lettow, Y. L. A. Rezus, A. Renn, G. Zumofen, E. Ikonen, S. Götzinger, and V. Sandoghdar, Quantum Interference of Tunably Indistinguishable Photons from Remote Organic Molecules, Phys. Rev. Lett. **104**, 123605 (2010).

[41] R. B. Patel, A. J. Bennett, I. Farrer, C. A. Nicoll, D. A. Ritchie, and A. J. Shields, Two-photon interference of the emission from electrically tunable remote quantum dots, Nat. Photonics **4**, 632 (2010).

[42] E. Flagg, A. Muller, S. Polyakov, A. Ling, A. Migdall, and G. Solomon, Interference of Single Photons from Two Separate Semiconductor Quantum Dots, Phys. Rev. Lett. **104**, 137401 (2010).

[43] M. Pompili, S. L. N. Hermans, S. Baier, H. K. C. Beukers, P. C. Humphreys, R. N. Schouten, R. F. L. Vermeulen, M. J. Tiggelman, L. d. S. Martins, B. Dirkse, S. Wehner, and R. Hanson, Realization of a multi-node quantum network of remote solid-state qubits, arXiv: 2102.04471 (2021).

[44] R. Trivedi, A. White, S. Fan, and J. Vučković, Analytic and geometric properties of scattering from periodically modulated quantum-optical systems, Phys. Rev. A **102**, 033707 (2020).

[45] V. M. Acosta, C. Santori, A. Faraon, Z. Huang, K.-M. C. Fu, A. Stacey, D. A. Simpson, K. Ganesan, S. Tomljenovic-Hanic, A. D. Greentree, S. Prawer, and R. G. Beausoleil, Dynamic Stabilization of the Optical Resonances of Single Nitrogen-Vacancy Centers in Diamond, Phys. Rev. Lett. **108**, 206401 (2012).

[46] L. De Santis, M. Trusheim, K. Chen, and D. Englund, Investigation of the Stark Effect on a Centrosymmetric Quantum Emitter in Diamond, arXiv: 2102.01322 (2021).